Constraining the Potential of the Milky Way using Stellar Streams

Timmy Ejdetjärn

Lund Observatory
Lund University

2017-EXA120

Degree project of 15 higher education credits
June 2017

Supervisor: Paul McMillan

Lund Observatory
Box 43
SE-221 00 Lund
Sweden

Abstract

The orbital approximation for stellar streams is the assumption that all stars in a stream can be described as following the same orbit. In this thesis, I evaluate this approximation as a method for constraining the potential of the Milky Way. I wrote a program in MATLAB which integrates the orbits of test particles in a potential model which resembles that of the Milky Way's halo and disc. The group of particles are set off with a velocity and position dispersion to act like a typical satellite. By varying the satellite's initial position, velocity and angle of the velocity relative to the disc, a large variety of different streams were created. The formed streams were treated as real observations, to determine how well the method works on actual streams. Using the position and velocity of the central particle in the satellite, orbits were fitted to the stream by altering the disc and halo masses and calculating the log-likelihood of each orbit. I try to constrain the mass values using a 90% confidence region in a 2D log-likelihood plot. The error in the orbital approximation is clearly visible when plotting the central orbit together with the simulated stream stars. No specific initial parameter (of the ones changed) gave a predictable confidence region, meaning that the approximation fails whatever the details of the stream models. It is found that most streams do not produce a confidence region that contain the masses of the potential they were actually created in. The percentage of confidence regions which had the actual masses inside them were 22.90%, which is very far from the 90% expected (from the confidence region) if the the orbital approximation was accurate. Only using streams with confidence regions entirely in the positive mass region gave a percentage of 12.50%. This means that past studies which used the orbit approximation are likely to have found incorrect answers regarding the shape and mass of the Milky Way.

Populärvetenskaplig beskrivning

Om dina ögon vore lika känsliga som astronomers toppmoderna teleskop skulle du kunna se långa band av ljus när du kollar upp mot himlen. Dessa band kallas stjärnströmmar och befinner sig i yttre delen av våran galax, Vintergatan. Strömmarna skapas från en klump av stjärnor, t.ex. en dvärggalax, medan de roterar runt Vintergatan. Det som händer är att stjärnor slits loss från klumpen och dras ut till en lång ström av stjärnor, som, i vissa fall, kan omfamna hela galaxen. Själva processen som drar ut stjärnorna till en lång ström är densamma som får månen att orsaka tidvatten på jorden; stjärnorna i klumpen som är närmre Vintergatan påverkas mer av galaxens gravitation och blir utdragna ur klumpen.

Det tog inte lång tid förrän astronomer kom på hur de kunde använda stjärnströmmar för att lära sig mer om Vintergatan. Exempelvis kan stjärnströmmar användas för att uppskatta galaxens massa, eftersom massan är relaterad till gravitationen som skapade strömmarna. Ett av sätten flera forskare använt för att ta reda på massan är att anta att alla stjärnorna i en stjärnström ligger på samma bana, dvs. stjärnorna följer efter varandra medan de roterar runt galaxen. Man vet att detta antagande inte är exakt rätt, men frågan är: hur fel är det?

I detta projekt undersöker jag ifall stjärnorna i en stjärnström verkligen kan sägas ligga på samma bana. Jag skriver kod och skapar ett program vilket tillåter mig att skjuta iväg en grupp partiklar i ett gravitationssystem, som ska föreställa Vintergatans. Efter att ha låtit partiklarna rotera runt ett tag bildar de stjärnströmmar och jag kan undersöka hur väl dessa följer en bana. Om banan och stjärnorna mestadels inte stämmer överens så vet vi att antagandet inte funkar. Målet är att göra detta för en massvis olika stjärnströmmar och avgöra ifall det finns specifika typer av strömmar för vilka antagandet kan användas.

Contents

List of Figures

List of Tables

Chapter 1

Introduction

The standard theory for structure build-up in the Universe is derived from the ΛCDM model, which is based on the idea that the Universe is dominated by cold dark matter (Madau et al. 2008). According to the model, the structures of a galaxy like the Milky Way originate from the hierarchical merging of smaller systems into larger ones. Accreted systems which do not merge with the galactic structure, become self-bound systems residing in the galactic halo. These are the substructures of a galaxy (referred to as subhalos and satellites) predicted by current theories and which are observed both in the Galaxy and simulations. There is one major discrepancy between simulations and observations; far fewer satellites have been detected in the Milky Way. This is known as the "missing satellites" problem (Moore et al. 1999; Klypin et al. 1999) and several solutions have been suggested. For example, it is possible that the missing satellites have yet to be seen, that there is something missing in the model or that the subhalos consist primarily of dark matter.

Stellar streams are disrupted satellites, e.g. dwarf galaxies and star clusters, in the halo of a galaxy. They are formed due to the tidal forces acting on satellites as they orbit around the galaxy. Several streams have been observed in the outskirts of the Milky Way and appear as long bands of stars across the sky. Belokurov et al. (2006) used photometric data from the Sloan Digital Sky Survey (SDSS), Data Release 5, to create an image of a part of the sky in which numerous streams reside. They called the region "The Field of Streams" and Figure 1.1 shows the region using Data Release 7 from the SDSS (GAIA-ESO Website 2013). Most notable is the Sagittarius (Sgr) stream, composed of stars from the Sagittarius dwarf galaxy, which was first discovered by Ibata et al. (1995). The Sgr stream is believed to wrap around the Galaxy and has multiple discernible substructures, e.g. the leading and trailing arm. The two branches of the Sgr stream, A and B, are thought to be stream debris from different time periods. A few other examples of streams in the Milky Way halo are the Monoceros ring (Newberg et al. 2002), the Orphan stream (named after its unknown origin) (Grillmair 2006) and the GD-1 stream (Grillmair & Dionatos 2006). As might be expected, satellites and streams have been observed in other galaxies as well; e.g. in the vicinity of Andromeda, Ibata et al. (2001) discovered a massive satellite and its stream, the giant southern stream (GSS).

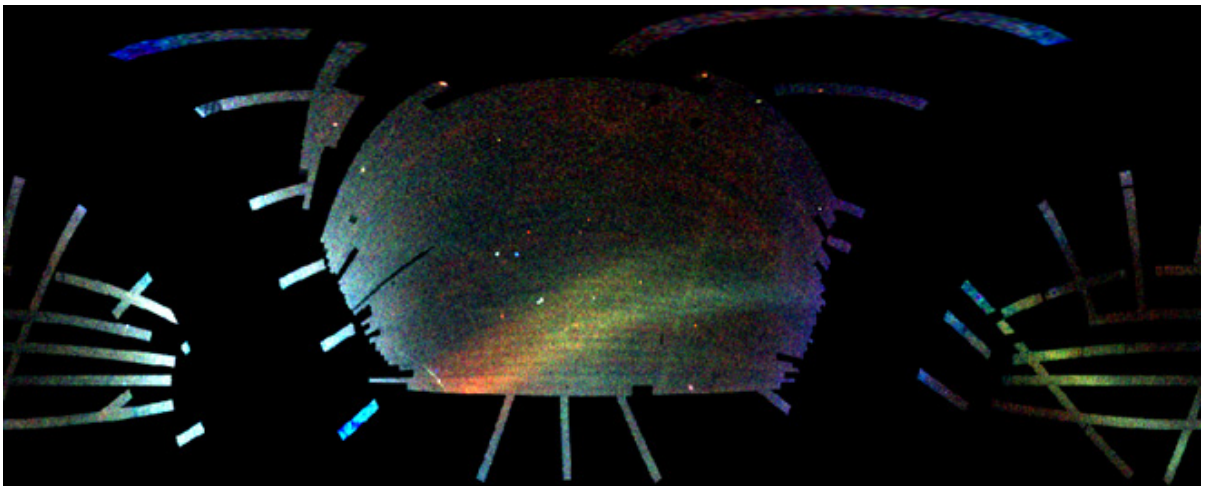

Figure 1.1: The Field of Streams, first imaged by Belokurov et al. (2006). The colours represent the distance to the stream stars, with red indicating distant stars and bluer colours for closer objects. The two adjacent, thick lines are the A and B branch (lower and upper, respectively) of the Sgr stream. The thin line passing through them is the Orphan stream. Source: GAIA-ESO Website

Stellar streams are powerful sources for determining properties of the Milky Way and its formation and evolution, since their progenitors were created together with the Galaxy and the streams formed from interaction with its potential. An application of observations of the streams is to establish the parameters which describe the gravitational potential of the Galaxy. Specifically, the total mass of the Galaxy is crucial to know, because galactic formation simulations dictate that a typical galaxy with a given mass should have certain characteristics. The missing satellites problem is an example of questions in cosmology which depend on whether the Milky way is a typical galaxy for its mass. Of course, the mass of the Milky Way needs to be known to answer this question.

Koposov et al. (2010) observed the GD-1 stream, created a 6D phase-space map of the stream (using data from SDSS, Calar Alto and USNO-B) and analysed the stars' positions, proper motions and radial velocities to constrain the gravitational potential of the Milky Way. Their main results were presented as the flattening of the total potential and the circular velocity at the Galactocentric distance of the Sun. They worked with the approximation that all the stars in a stream follow the same orbital path, which is useful because it reduces the complexity of the problem to one orbit. The approximation is known to be incorrect from how streams form; the stars need to be on separate orbits for a stream to form after the tidal forces tear the satellite apart. It was still believed to be a reasonable approximation, since the stream stars all have similar orbits. A specific orbit arises only for a particular potential. Given an orbit, the potential can be ascertained; represented by a certain set of (galactic) parameters. By fitting an orbit to the GD-1 stream, Koposov et al. determined the range of these parameters with a 90% confidence. The GD-1 stream was chosen because it is a long and thin stream and, in contrast to

previous constraints (using the orbital approximation) on the wider Sgr stream (Law et al. 2005; Johnston et al. 2005), a thinner stream would result in a better fit, which translates into more precise values (according to Koposov et al.). A thin stream is formed from a satellite with relatively low internal energy, meaning most stream stars have similar velocities, which makes the orbital approximation seem appealing. Despite it sounding correct, the accuracy of the approximation needs to be established.

In this project, I aim to use a similar method as the one used by Koposov et al. to constrain the gravitational potential of the Milky Way, but with focus on determining the viability of the orbital approximation for stellar streams. The major difference is that I will write a computer simulation to create several streams and then treat them as real observations. By evaluating streams formed from satellites with different properties (e.g. initial values), I hope to ascertain if there are particular cases for which the orbital approximation holds. In Chapter 2, a model potential is introduced to emulate the potential of the Milky Way. The treatment of this potential, in order for particles to form orbits in the simulations, is also shown. Additionally, Chapter 2 involves the fitting method of an orbit to the stream and how the values are constrained with a confidence region. Chapter 3 demonstrates how the streams were formed during the simulations and examples of the fitting and confidence region. The relevant data found for the streams is revealed in multiple tables and discussed. Finally, Chapter 4 explains what can be said about the orbital approximation for stellar streams, what else can be done and how it relates to e.g. galactic formation. At the end of the Chapter, a link is given to the code I produced.

1.1 The Milky Way

The Milky Way is generally identified as a barred spiral galaxy, by the Hubble classification. The three characteristics of a spiral galaxy are the bulge, disc and halo. The bulge is the massive, galactic centre (GC) of the Galaxy, made out of stars which extend into a bar-like structure, but is also believed to contain a supermassive black hole in the middle. The disc is the flat plane of gas clouds and stars surrounding the bulge, forming a spiral arm structure. The halo enwraps the entire Galaxy, stretching out well beyond the disc, and it is in the outer halo where most satellites and, by extension, streams reside. The halo consists dominantly of dark matter, which can not be directly detected, but is inferred by the constant rotational speed of certain objects in the Galaxy. The high speeds observed at large distances are explained by the, roughly spherical, dark matter halo (e.g. Phillips 2005).

Chapter 2

Method

2.1 Units

SI units can be inconvenient when working with the masses and distances associated with stars and galaxies. Expressing the unit of mass in terms solar masses $M_\odot$, the distance in parsecs [pc] and velocity in km/s, the gravitational constant can be written

$$G = 0.004301 \text{ pc } (\text{km/s})^2 \, M_\odot^{-1}$$

and the unit of time becomes

$$1 \text{ pc}/(\text{km/s}) = 0.9778 \text{ Myr}.$$

2.2 The Galactic Coordinate System

The galactic coordinate system is based on the location of the Solar system in the Milky Way (evaluated in this project to be 8 kpc from the GC), making it frequently used when examining objects inside the Galaxy. The coordinates are: the galactic latitude b, which is the angle from the disc plane, and the galactic longitude ℓ, the angle in the plane from the GC (increasing in the opposite direction of the galactic rotation) (e.g Lindegren 2014). Both angles are expressed in degrees. The galactic coordinates together with the distance (from the Sun) $r_\odot$ to the observed object give its exact position in the Galaxy.

The primary coordinates used in the simulation process are galactocentric Cartesian (x, y, z) coordinates. The Cartesian coordinates were made heliocentric and then transformed into the galactic coordinates.

2.3 The Modelled Potential

The gravitational potential of the Milky Way is represented by the aforementioned (section 1.1) components in a spiral galaxy. This project concerns the Galaxy's satellites and,

therefore, only the potential from the disc and halo are considered when modelling the potential, as the bulge should have a negligible contribution at typical stream distances. The Milky Way disc is regarded as being homogeneous and has an axisymmetric, highly flattened potential, which can be described by a Miyamoto-Nagai potential (Miyamoto & Nagai, 1975), shown below.

$$\Phi_{\text{disc}} = -\frac{GM_{\text{disc}}}{\sqrt{(x^2 + y^2 + (a_{\text{disc}} + \sqrt{z^2 + b_{\text{disc}}^2})^2)}}, \tag{2.1}$$

where the scale height and width for the Milky Way are $a_{\text{disc}} = 3.7$ kpc and $b_{\text{disc}} = 0.2$ kpc, respectively, and are representative of the size and shape of the disc. The disc and halo masses M_{disc}, M_{halo} are treated as free variables during the simulation.

The potential of the halo is assumed spherically symmetric and given by a Hernquist potential, which can be derived from the Hernquist model density distribution (Hernquist 1990), found in e.g. Binney & Tremaine (2008), to be

$$\Phi_{\text{halo}} = -\frac{GM_{\text{halo}}}{r + a_{\text{halo}}}. \tag{2.2}$$

The scale radius of the halo's potential, $a_{\text{halo}} = 18.5$ kpc was treated as a free variable when fitting for a few simulations (more discussed in Section 3.4).

The total potential exerted on an object sum in the same way as for the total force. This can be derived from forces being added linearly and the potential simply being the integral of the gravitational forces (as seen in Eq. (2.4)). The total potential of the Galaxy is then merely the addition of the two components,

$$\Phi_{\text{tot}} = \Phi_{\text{halo}} + \Phi_{\text{disc}}. \tag{2.3}$$

2.4 Applying the Potential

2.4.1 Equations of Motion

The force referred to in this project is per mass unit, also called specific force. The force is then evidently equivalent to the acceleration, which simplifies relevant equations by getting rid of the mass of individual particles. The acceleration of a test particle in a potential $\Phi(x, y, z)$ can then be determined from the derivative of the potential along the individual coordinates, as shown below.

$$\vec{a} = \begin{cases} \dfrac{\mathrm{d}^2x}{\mathrm{d}t^2} = -\dfrac{\partial\Phi}{\partial x} \\ \dfrac{\mathrm{d}^2y}{\mathrm{d}t^2} = -\dfrac{\partial\Phi}{\partial y} \\ \dfrac{\mathrm{d}^2z}{\mathrm{d}t^2} = -\dfrac{\partial\Phi}{\partial z} \end{cases} \tag{2.4}$$

As the potential is dependent on all three directions, the three second-order ordinary differential equations (ODE) need to be solved simultaneously. For numerical integration, this is accomplished by re-writing them as six first-order ODEs. The velocities (u, v, w) are naturally the derivative of the positional coordinates, which gives the following set of ODEs.

$$\begin{cases} \dfrac{\mathrm{d}x}{\mathrm{d}t} = u \\ \dfrac{\mathrm{d}y}{\mathrm{d}t} = v \\ \dfrac{\mathrm{d}z}{\mathrm{d}t} = w \\ \dfrac{\mathrm{d}u}{\mathrm{d}t} = -\dfrac{\partial \Phi}{\partial x} \\ \dfrac{\mathrm{d}v}{\mathrm{d}t} = -\dfrac{\partial \Phi}{\partial y} \\ \dfrac{\mathrm{d}w}{\mathrm{d}t} = -\dfrac{\partial \Phi}{\partial z} \end{cases} \tag{2.5}$$

We can solve these ODEs if the initial position and velocity of the particle are given. (e.g. Lindegren 2014)

2.4.2 MATLAB ODE45

The programming is done in MATLAB and uses their built-in solver for ODEs, ode45. There are several different versions for the integrator, denoted by the number in its name. The ode45 is an all-purpose ODE solver, viable for most problems. It applies a specific Runge-Kutta method for solving the equations, provided the start variables, e.g. written in the form $W = (x_0, u_0, y_0, v_0, z_0, w_0)$, and the time interval. If a timestep is not specified then ode45 will alter the timestep while integrating; for efficient computation (MathWorks Website 2017).

2.4.3 Circular Velocity

The velocity needed for the orbit to be circular in a potential is found by balancing the gravitational and centripetal force. The circular velocity can then be calculated from

$$\frac{v_\mathrm{c}^2}{r} = \left| \frac{\partial \Phi}{\partial r} \right|. \tag{2.6}$$

The circular velocity is useful when assigning initial velocities to the objects in the potential. Choosing a velocity near the circular velocity is a convenient choice because the satellite will not escape nor "fall" into the potential for these velocities.

2.5 Fitting method

The approximation that stellar streams follow an orbital path entails that every individual stream star follows the same orbit. Simply fitting a line that contains most of the stream stars and calling this their orbit does not work, since the velocities of the individual stream stars are not considered. The central particle is in the satellite's centre and has no peculiar velocity, so it should the best representation of the satellite as a whole; the average position and velocity of all particles equals that of the central particle. We decide on using the position and velocity of the central particle for the fitting process, with the assumption that these values are exactly known from observations. This is a reasonable approximation because the velocity of the satellite that is being stripped can be determined very accurately from combining observational data from stars in the stream. Using the velocity and position of this central particle at the time the stream is observed, yields the orbital path of the particle when integrated forwards and backwards in time. By changing the disc and halo mass, the potential is altered until the best fit of the model to the stream is achieved. If streams really follow an orbit (as in the approximation by Koposov et al.) then this would be the actual potential of the Galaxy.

2.5.1 Orbit likelihood fitting

The likelihood that a stream star fits the modelled stream orbit is a comparison between the position of the star and the model, represented by normal distributions. This is a statistical approach, which necessitates an uncertainty in the values. Since there are no systematic errors in a simulation, the values used for the uncertainties used are found on observational errors. The simulated stream stars were treated as real observations. Therefore, the normal distributions contained the variables in the galactic coordinate system. The latitude and distance of the stream stars were treated as functions of the longitude ℓ; hence, there are values for each longitude. Then, for a given ℓ there is a likelihood for a stream star to be part of the stream model, as shown in the equation below. This method assumes there is only one star per ℓ value.

$$\begin{aligned} P(b, r|\ell) = &\frac{1}{\sqrt{2\pi\sigma_b^2}}\exp\Big(-\frac{1}{2}\left(\frac{b_{\text{model}} - b}{\sigma_b}\right)^2\Big) \\ &\times \frac{1}{\sqrt{2\pi\sigma_r^2}}\exp\Big(-\frac{1}{2}\left(\frac{r_{\text{model}} - r}{\sigma_r}\right)^2\Big), \end{aligned} \tag{2.7}$$

where the uncertainties are $\sigma_b = 1^\circ$, which is an estimate of the stream width, and $\sigma_r = 3$ kpc, a typical uncertainty in distance; in reality, it changes with the distance to the observed object.

Multiplying these probabilities for every star gives the total likelihood that the model fits the stream. Maximising this probability, by modifying the potential, results in the potential parameters which give the best fit. The logarithm of the likelihood, log-likelihood,

is used to avoid numerical problems caused by the magnitude of the total probability becoming minuscule. The total log probability for a given ℓ that the model fits the stream is

$$\log P = \sum_{i=1}^{n} \Bigg(\log \frac{1}{\sqrt{2\pi\sigma_b^2}} \exp\Big(-\frac{1}{2}\left(\frac{b_{\text{model}} - b_i}{\sigma_b}\right)^2 \Big) + \log \frac{1}{\sqrt{2\pi\sigma_r^2}} \exp\Big(-\frac{1}{2}\left(\frac{r_{\text{model}} - r_i}{\sigma_r}\right)^2 \Big) \Bigg), \tag{2.8}$$

where the index i denotes a specific star. The fitting is based on finding the highest log-likelihood for the two functions, displayed for an example stream in Figure 2.1.

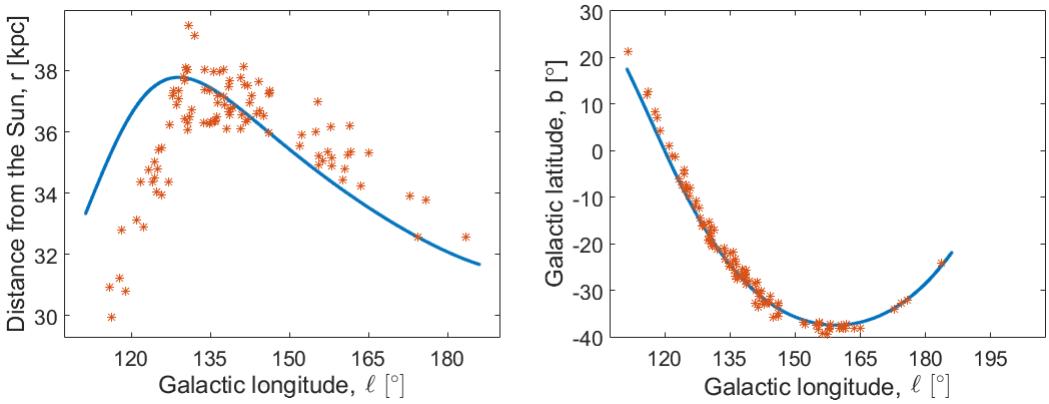

Figure 2.1: An example of the two functions fitted for orbits to a stream. Distance to the Sun as a function of the longitude (left graph) and the latitude as a function of the longitude (right graph). The lines are the values for the orbit models and the asterisks '*' are the simulated stream stars.

2.5.2 Confidence Region

Because the fitting is statistical, it is possible for the actual value to not be the most probable one. A confidence region (CR) is a region where there is a pre-established confidence that the actual value must be a part of it. The region is defined as the range the probabilities have to lie within, around the maximum likelihood P_{max}, for a certain confidence level to be achieved. The CR size and shape changes depending on the confidence level and the degrees of freedom. In this project, a 90% CR is established for a 2D likelihood plot, since we have two free variables (halo and disc mass). The log-likelihood is then defined to lie within the range

$$\log P > \log P_{\text{max}} - 2.30 \tag{2.9}$$

in order for us to have a 90% confidence that the actual disc and halo mass are inside the CR (e.g. Lindegren 2016). An example of how a typical confidence region is displayed in this project can be seen in e.g. Figure 3.4.

The CR can be used to constrain the gravitational parameters by inspecting the values at the borders of the region. This will only provide accurate results if the orbital approximation works, since the likelihoods calculated are derived from a single orbit. There is no definitive method to assess if the approximation is inaccurate from looking at the CR. However, even though the actual values might still be inside the CR, if the approximation is not valid then they are not expected to consistently be within it. By judging from several log-likelihood plots, it should become evident if the actual values do not fall into the CR ninety percent of the time.

Chapter 3

Results

3.1 Creating Streams

In the simulation, streams were formed from a hundred test particles spherically distributed, formed from randomly generated normal distributions in each of the three Cartesian coordinates. The radius of the sphere was 0.1 kpc, as it is a typical size of a satellite. The central particle of the satellite was given an initial position and velocity v_0, which were altered to create a variety of streams. The initial position r_0 was set in the disc plane and the initial velocity had an angle θ relative to that plane. The Galactocentric distance of streams can vary substantially, but most of the streams presented were created at $r_0 = 12$ kpc, which corresponds to $v_c(12 \text{ kpc}) = 189$ km/s. The angle was changed with a 15° interval, not including 0° or 90° (because these values formed unnatural streams which have not been observed); i.e. 15°, 30°, 45°, 60°, 75°. The magnitude of the velocity was varied relatively near the circular velocity for the distance of the initial position. The particles surrounding the central particle were assigned a similar initial velocity, but with a normally distributed peculiar velocity added (set as maximum five percent of the circular velocity) to emulate the behaviour in an actual satellite. The peculiar velocities were also meant to reflect that we did not know these velocities exactly.

There is no handling of the gravitation between stars in the satellites, as the satellites are considered to have already become disrupted and are not gravitationally bound any more. The satellites are therefore treated as having become disrupted just as the simulation starts, which can be explained by the disruption taking place from a single event (and not over a period of time). Placing the satellite in the disc can be justified as disc shock - disruption from passing through the disc. The orbit of each particle was found by integrating their coordinates over a period of time. As the integration time is increased, the satellite gets more stretched out and starts looking like a typically observed stream. This is viewable in Figure 3.1, along with the orbital path of the central particle as a comparison between the orbital approximation and the position of the simulated stream stars. For some of the integration times shown the stream seemingly follows the orbit, while for others the orbit and stream massively differ; making it a faulty approximation. The inaccuracy of the

assumption that the particles follow the same orbit is made obvious in Figure 3.2, where each individual orbit is plotted for 10 particles. Shown in one plane (the x-y plane) so to reduce the number of images presented.

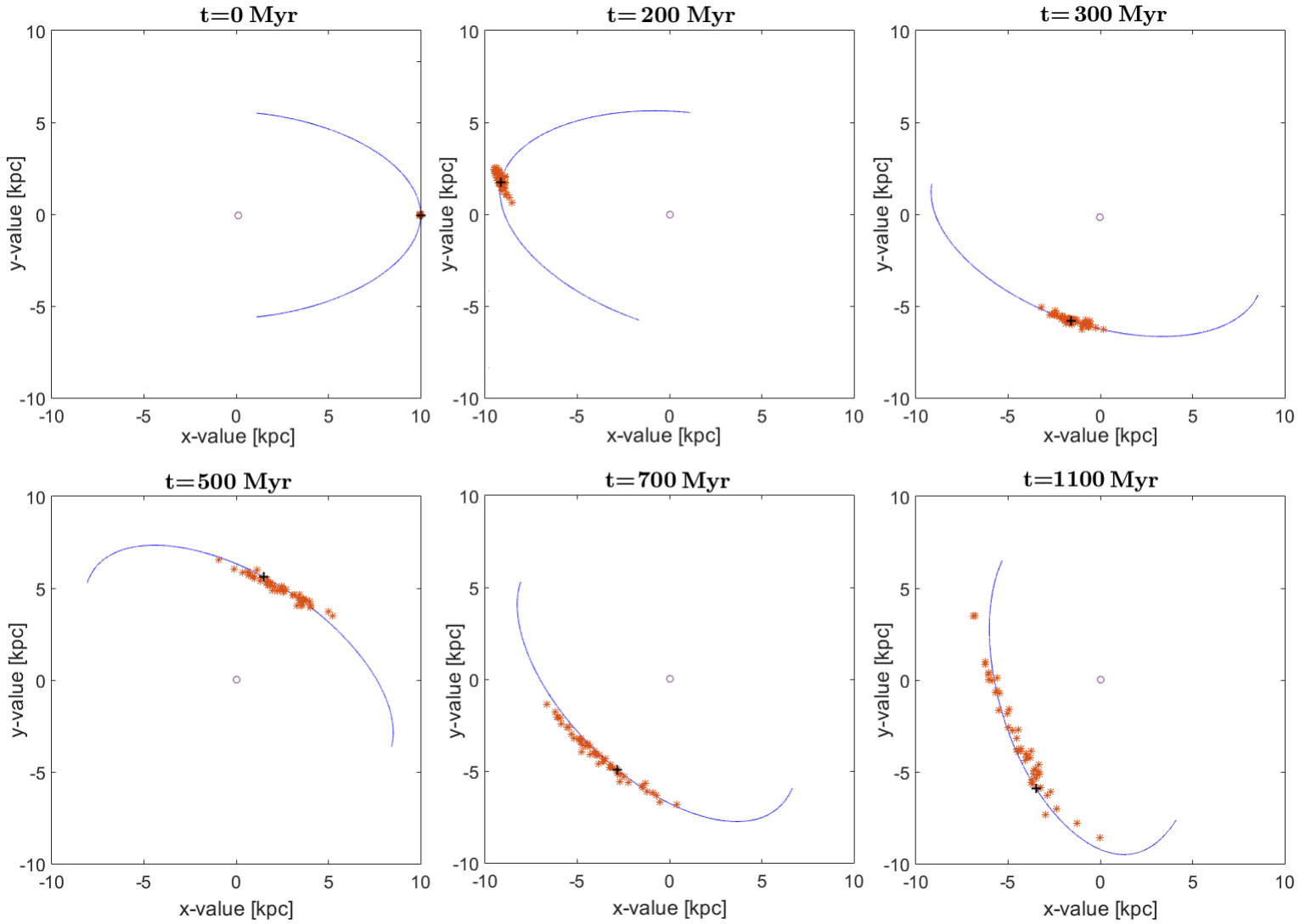

Figure 3.1: 2D images from the simulation of the stream creation process, showing how it takes form with the increasing integration time t. The asteriks '*' represent the stars in the satellite/stream and the plus sign '+' marks the centre of the satellite. The GC is represented as the 'o'. The curve shown is the orbit of the central particle near its current position.

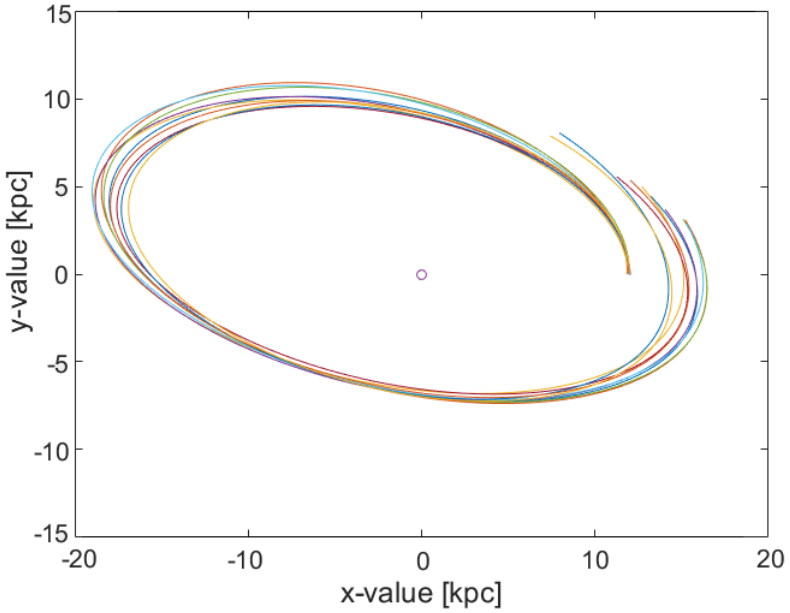

Figure 3.2: The orbits for a satellite of ten particles displayed in 2D for a full lap. The orbits are clearly spreading out and do not follow a single orbit. A peak separation of around 3 kpc between orbits can be measured.

3.2 Fitting Stream Orbits

Figure 3.4 and 3.5 show examples of two different streams and the log-likelihood plots produced from fitting orbits to them. Each figure has two different graphs of the stream, one with the orbit of the central particle and the other with the best fit orbit. Figure 3.4 shows the orbital approximation follows the stream well in the x-y plane, when judging by eye, while the other Figure 3.5 shows the results when the orbital approximation is clearly not viable. The best fit that could be achieved for this stream still does not contain all the stream stars, however, this confirms that the stream can not be described by an orbit with the velocity and position of the central particle. The coloured parts in the likelihood plots are all within the 90% CR and the colours correspond to different log-likelihood values. Since the fitting method only involves achieving the best fit, the CR may contain negative mass values as long as the fit is good. However, negative mass is unphysical so the plots used are cut off at zero mass for both components and the area below is discarded. With the 90% CR as defined above in Eq.(2.9), we can not be certain that this is a completely fair approximation when the CR is cut off. Nevertheless, this approximation is applied to the CR throughout the project.

The significance of some set parameters for the CR was investigated. First off, the randomly generated velocity and position dispersions appear to affect the CR significantly when integrating a stream several times using the same initial conditions. The CR "jumps

around" on the likelihood plot and the area marginally changes, as seen for one example in Figure 3.3. Increasing the number of particles used for the simulation was found to slightly decrease the area of the CR, but the jumping around of the CR did not. However, longer integration times diminished the CR moving. These conclusions were motivated by the values in Table A.1 and show that 100 particles have a CR similar to 200 particles. The obvious advantage of fewer particles is that it corresponds to less simulation time.

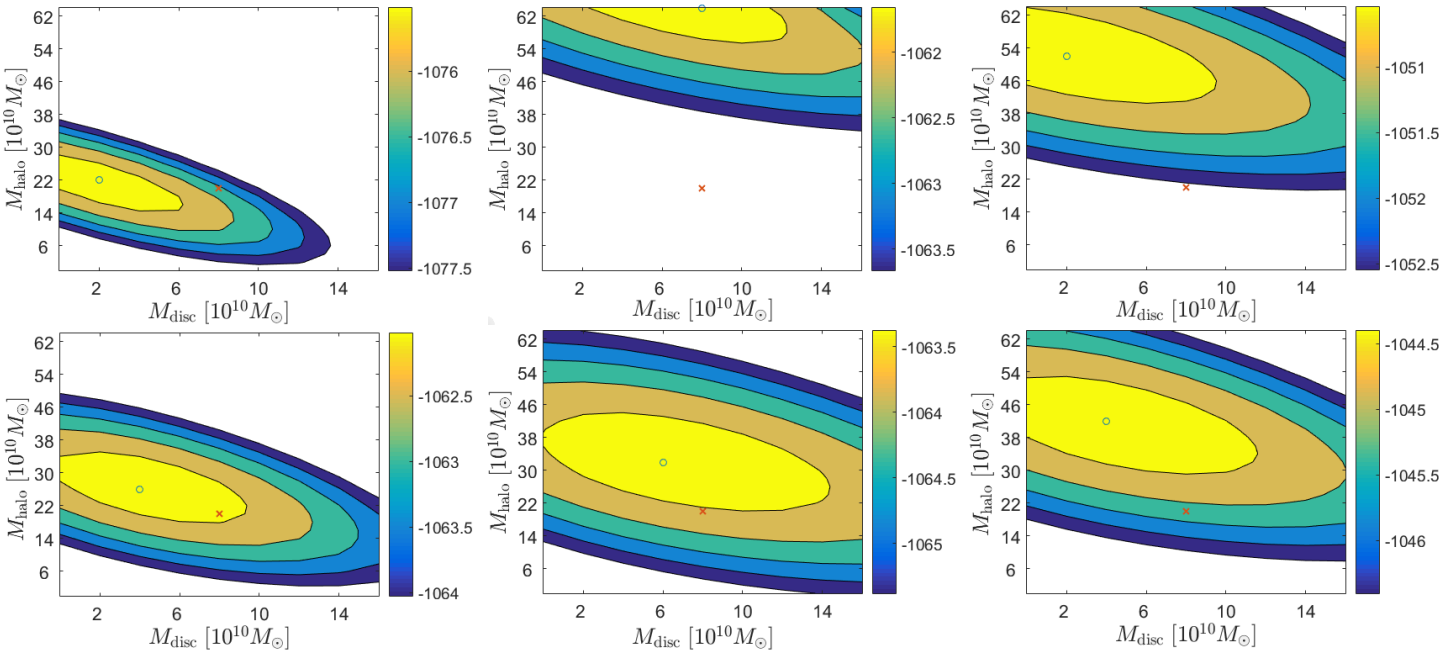

Figure 3.3: The CRs from integrating 100 particles with the same initial conditions, meaning the only difference is how the velocity and position of particles are randomly distributed. It is worth mentioning that these examples are for an early stream with a big CR area.

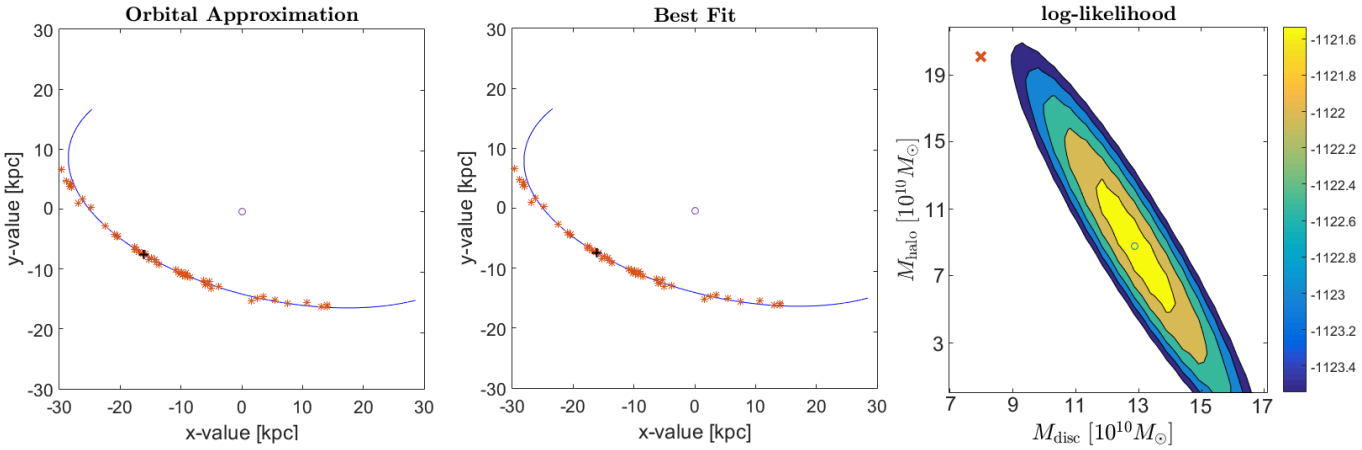

Figure 3.4: The image to the left displays a stream where the orbit of the central particle seemingly contains most stream stars. The middle images shows the best fit for the stream, corresponding to the masses found in the log-likelihood plot (to the right) marked by 'o'. The 'x' in the log-likelihood plot points at the actual values.

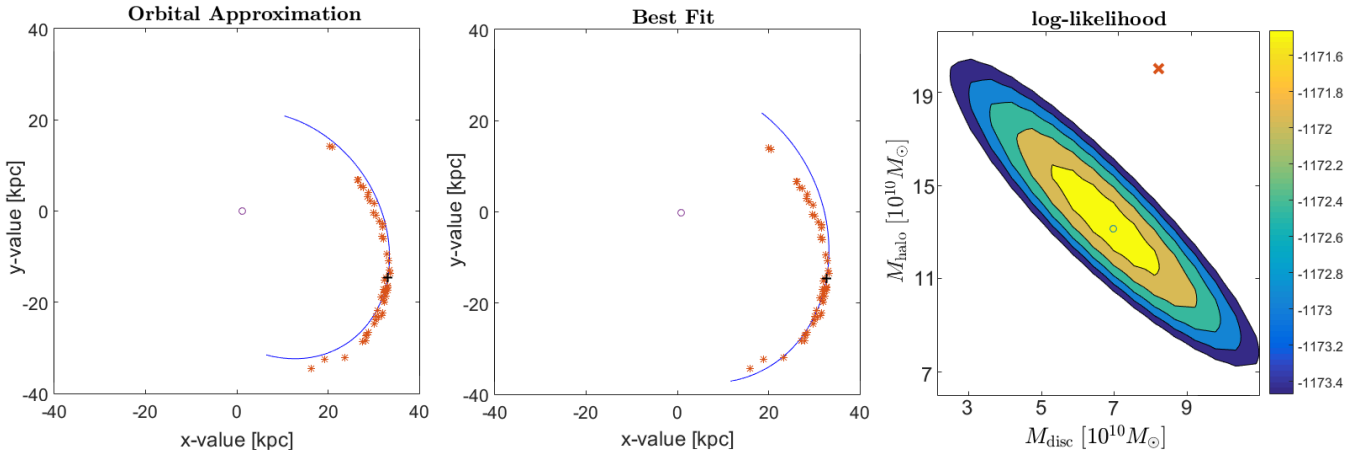

Figure 3.5: The image to the left displays a stream (in 2D) where the stream stars do not fall on the orbit of the central particle. The middle image shows the best fit for the stream, corresponding to the masses found in the log-likelihood plot (to the right) marked by 'o'. The 'x' in the log-likelihood plot points at the actual values.

3.3 Quantifying Fitting Results

All the streams were created in a potential with known disc and halo masses and reasonably the CR should centre around, or at least contain, these "true" values. For all results presented, these masses were $M_{\text{disc}} = 8 \cdot 10^{10} M_\odot$ and $M_{\text{halo}} = 20 \cdot 10^{10} M_\odot$. For example, Figure 3.4 and 3.5 highlight the actual masses and those which gave the best fit. The figures demonstrate that the masses differ noticeably for both, even though one seems to follow

the orbital approximation. The best fit parameters and whether or not the actual value is in the 90% CR are therefore important when evaluating the streams. Another noteworthy property is the area (unit $[(10^{10}M_{\odot})^2]$) of the confidence region (for masses above zero), because it is directly related to how precise the fit is. These significant variables of the stream fitting are used to represent the streams in the tables below.

The integration time used for the streams does not have a set interval. Instead, it is decided to be from when the simulated stars first form a recognisable stream until the stream has stretched about half a lap around the galaxy, which is usually when the CR became too small to evaluate. Neither do the streams in the tables use the same integration time, because some stream models give maximum log-likelihoods (and CR) that are at very negative masses for one or the other component. This means that the peak values are distant from the actual values and the area in the positive region is zero. This type of data is not useful when trying to find out if and how the different stream variables relate to each other. However, they are still of use when determining how many streams contain the actual values. It is also important to note that when a model gives results so far from the true values (we do not even consider them to be physical), it is further evidence that the orbit fitting approach is not correct.

3.3.1 Varying Initial Angle

Distance 12 kpc

Table 3.1: The relevant parameters for streams created at $r_0 = 12$ kpc with constant initial velocity $v_0 = 1.2v_c$ and a range of angles, observed at different times. The masses presented are for the best fit.

θ [°]	t [Myr]	CR area	In 90% CR?	M_{disc} $[10^{10}M_\odot]$	M_{halo} $[10^{10}M_\odot]$
15	600	1200	No	13	60
	1000	170	Yes	5	35
	1300	96	No	15	27
30	600	584	Yes	8	22
	1000	82	No	2	60
	1300	5	No	7	39
45	800	525	Yes	7	22
	1000	160	No	3	70
	1400	3.5	No	14.0	3.5
	2200	2.5	No	14	2
60	500	300	No	2	110
	950	117	No	12	2
	1250	37	No	2	21
	1580	50.5	No	8.5	28.0
75	500	844	No	22	3
	960	2	No	16	-19
	1560	66.8	No	3.5	42.0

I varied the angle of the initial velocity, while keeping the speed constant, for a satellite at the initial distance 12 kpc. The values for these streams are presented in Table 3.1. In the x-y plane, I noticed that the streams created seemed to form a coherent line of stars that got slightly more spread out as the angle was increased. In the x-z plane, both low and high angles were spread out; higher angles more than lower. Both planes are shown for streams created from three different initial angles (at high integration times) in Figure 3.6. Since the modelled halo potential is spherically symmetric, the change in stream values for different angles is caused by the disc potential. A stream very close to the disc plane (small angle) is more strongly and uniformly affected by the disc potential; it gets wider in the z-direction but is still around the central orbit. Larger angles have one side of the stream getting pulled more than the other, effectively tearing away stars. The difference in the effects can be seen in the figure, but it is difficult to predict how these would affect the CR. At most, the 75° stream looks harder to fit an orbit to. The stream data does not help identifying any relation between variables, except for the area decreasing with time (which is further discussed in Section 3.3.3). The lack of actual values in the CRs is investigated in Section 3.3.4.

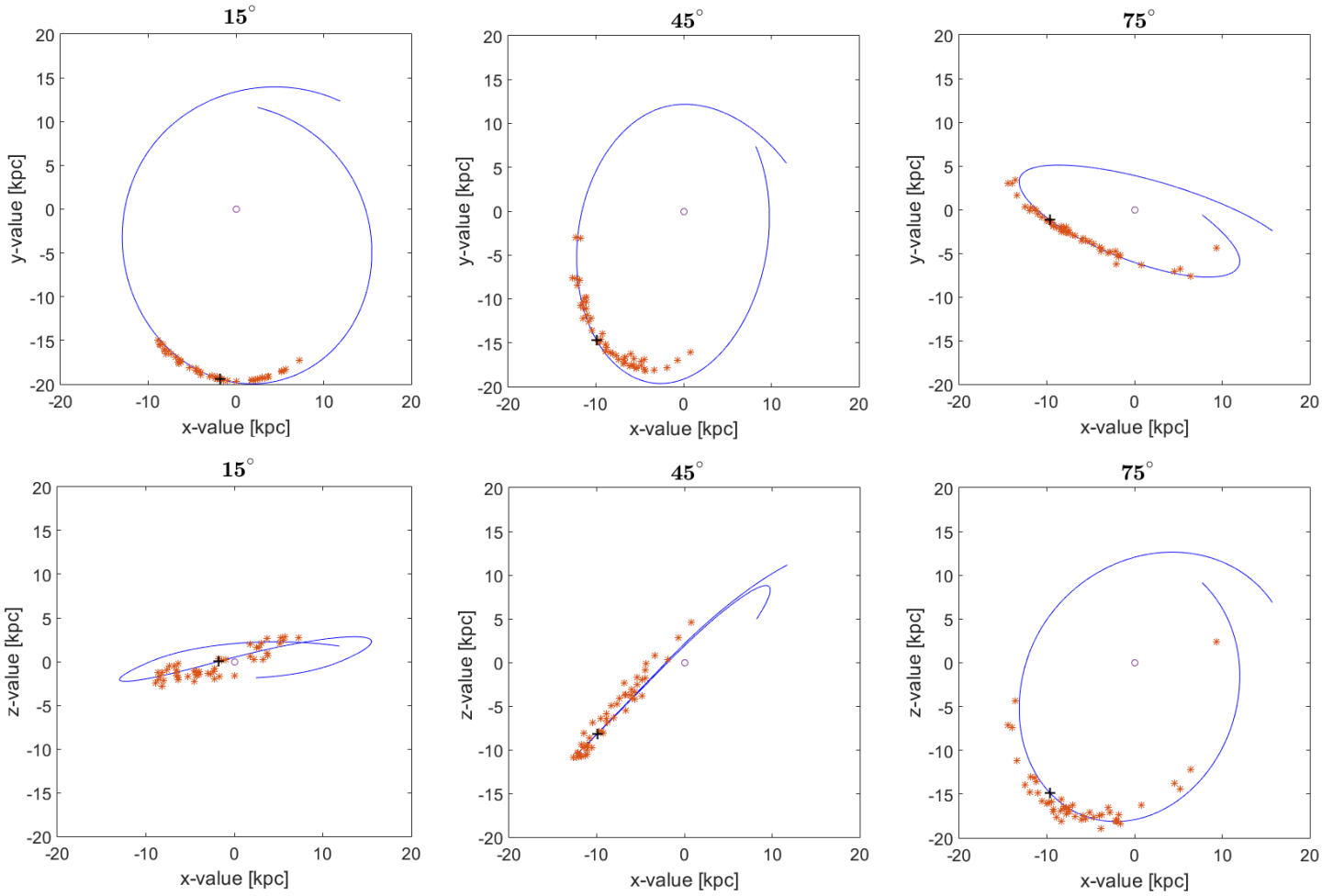

Figure 3.6: Orbits in the x-y and x-z plane for three streams with different angles and the same velocity $1.2v_c$. The line is the central orbit, the asterisks '*' are the stream stars and 'o' the GC.

Distance 24 kpc

Table 3.2: The relevant parameters for streams created at $r_0 = 24$ kpc (corresponding to $v_c(24 \text{ kpc}) = 159$ km/s) with constant initial velocity $v_0 = 1.2v_c$ and a range of angles, observed at different times. The masses presented are for the peak log-likelihood.

θ [°]	t [Myr]	CR area	In 90% CR?	M_{disc} $[10^{10}M_\odot]$	M_{halo} $[10^{10}M_\odot]$
15	1300	348	No	4	54
	1800	750	Yes	12	12
	2600	100	No	7	33
	3400	94	Yes	12	8
	3800	24	No	7	25
	4300	51	No	12	9
	4800	22	No	11	21
30	1300	516	No	16	25
	1800	820	Yes	8	34
	2400	46.8	No	11.5	8
	2800	236	No	2	42
	3400	54	No	15	3
	4300	92.5	No	4.5	22.0
	4600	16.3	No	9.5	9.0
	4800	13.5	No	18.0	2.5
45	1300	568	No	10	42
	2500	58	No	15	7
	2800	192	No	6	48
	3400	40	No	9	12
	4100	48	No	17	6
60	1300	476	No	10	30
	2000	133	No	34	-20
	2500	74	No	14	5
	3400	61	No	11	8
75	1300	484	No	12	40
	2500	80	No	6	38
	2700	120	Yes	4	32
	3400	33	No	14	6
	4100	24.8	No	14.5	3.5

The angle was altered for a constant velocity for a satellite at the initial distance 24 kpc. The stream results are presented in Table 3.2. The first thing to be noted is that there are many more values in this table than Table 3.3, which is simply because it was easier for me to find streams which had a CR around the positive mass region for this initial distance. This implies that a distance further away gives more reasonable values than closer values.

I observed that the streams with a large initial angle have stars slightly more spread out from the stream; I refer to Figure 3.6 from before. With the disc being further away, the total potential felt by the streams should be more spherically symmetric, meaning the angle matters less. Evidently, there is still a difference between angles for the same integration time as the stream values are not the same. Once again, the area is seen decreasing, but at some points it increases. The integration time and 90% CR is discussed more in-depth in Section 3.3.3 and Section 3.3.4, respectively.

3.3.2 Varying Initial Velocity

Table 3.3: The relevant parameters for streams created at $r_0 = 12$ kpc with constant angle $\theta = 45°$ and a range of initial velocities, observed at different times. The masses presented are for the peak log-likelihood.

v_0 [v_c]	t [Myr]	CR area	In 90% CR?	M_{disc} [$10^{10} M_\odot$]	M_{halo} [$10^{10} M_\odot$]
0.9	520	324	No	12	-14
	1000	50	No	17.2	17.2
1.0	650	1000	Yes	10	38
	700	100	No	24	20
	950	0.8	No	14.5	0.3
	1300	6.7	No	16.5	9.0
1.1	700	308	No	2	42
	1150	14.3	No	6.5	33.0
	1450	4.3	No	11.0	3.0
	1600	7.1	No	6.5	39.0
1.2	800	525	Yes	7	22
	1000	160	No	3	70
	1400	3.5	No	14.0	3.5
	2200	2.5	No	14	2
1.3	600	130	Yes	4	49
	1040	640	Yes	6	18
	1250	35.1	No	8.5	28.0

The velocity of the central particle was altered near the circular velocity at a constant angle. The values for these streams are presented in Table 3.3. Figure 3.7 shows the x-y and x-z planes of three example stream at high integration times. I observed that the satellites with a high velocity formed rather narrow streams compared to low velocity streams, which had stars more spread out. The satellites with a speed lower than the circular velocity orbited closer to the GC and are therefore closer to the centre of the potential, which could cause the spreading. Due to the closer orbit, these streams also travel through the disc more often, which could contribute to tearing them apart and appear wider. Another factor could be that the peculiar velocity has a bigger impact when the stars in the satellite have

a lower velocity (dispersion is relatively larger). These observations can not be seen in the stream values and neither can any other clear relation be deducted from the data. The exception to this is the area decreasing with time, discussed in Section 3.3.3.

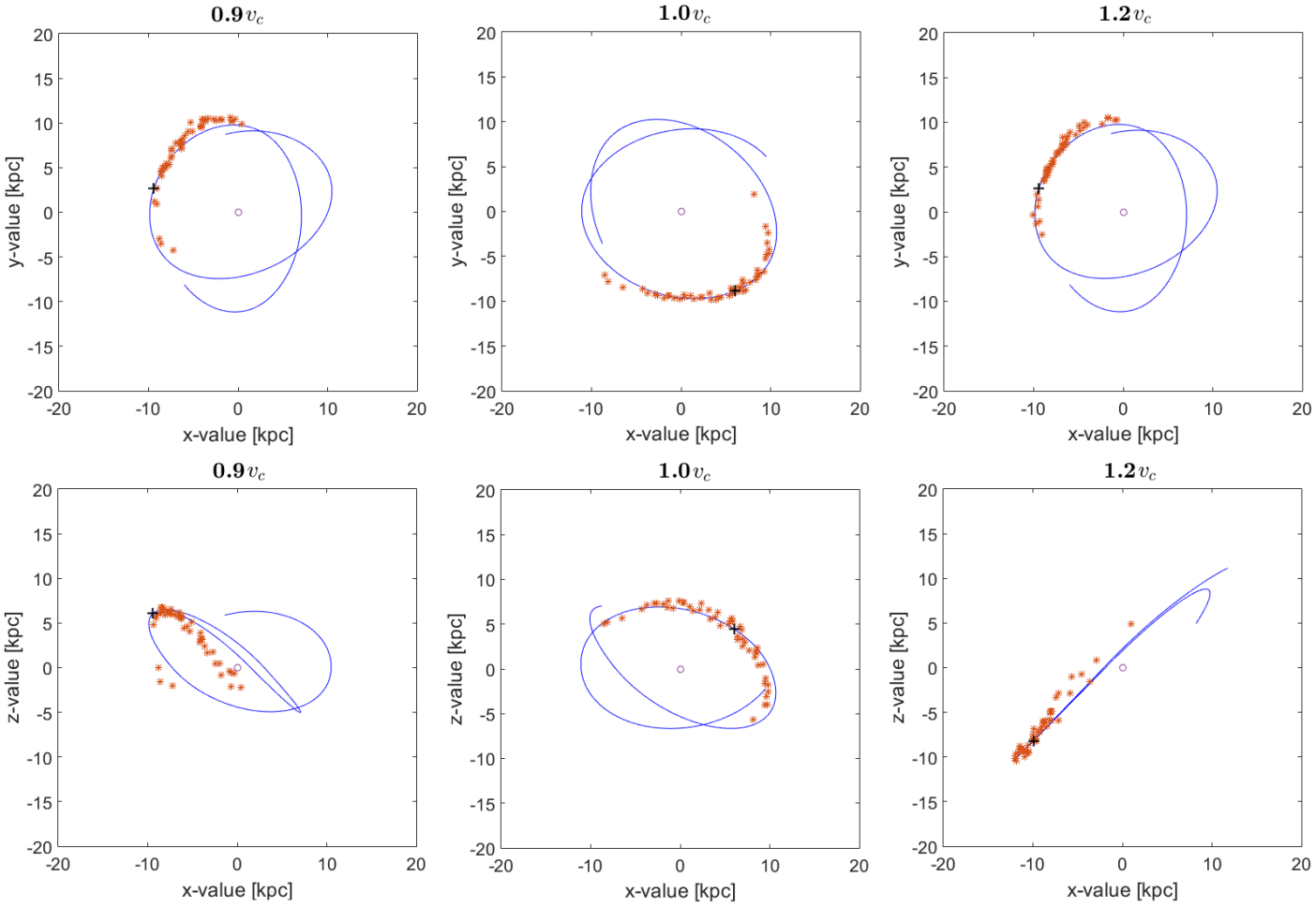

Figure 3.7: Orbits in the x-y and x-z plane for three streams with different velocities and the same angle 45°. The line is the central orbit, the asterisks '*' are the stream stars and 'o' the GC.

3.3.3 Increasing Integration Time

Using the tables for the different streams above, a solid trend is clear: the area of the CR decreases with time. This relation is logical, as time passes the stream gets further dragged out and the fitting becomes more precise. An especially clear example of how the area decreases is shown in Figure 3.8. The area over time can be seen having bumps, increasing for one specific time then decreasing again. This is just attributed to the streams becoming wider at certain points in time, possibly due to when passing through the disc. The integration time is equivalent to the time at which the stream is observed. Almost

all streams with a low integration time have a large CR area, which makes sense since the early streams are very wide. What can be seen in both figure and data is that the CR does not just become narrower, it also changes position outside of the previous CR. This is additional proof that the orbit fitting method is not a viable approximation; the potential derived changes depending on when the stream is observed.

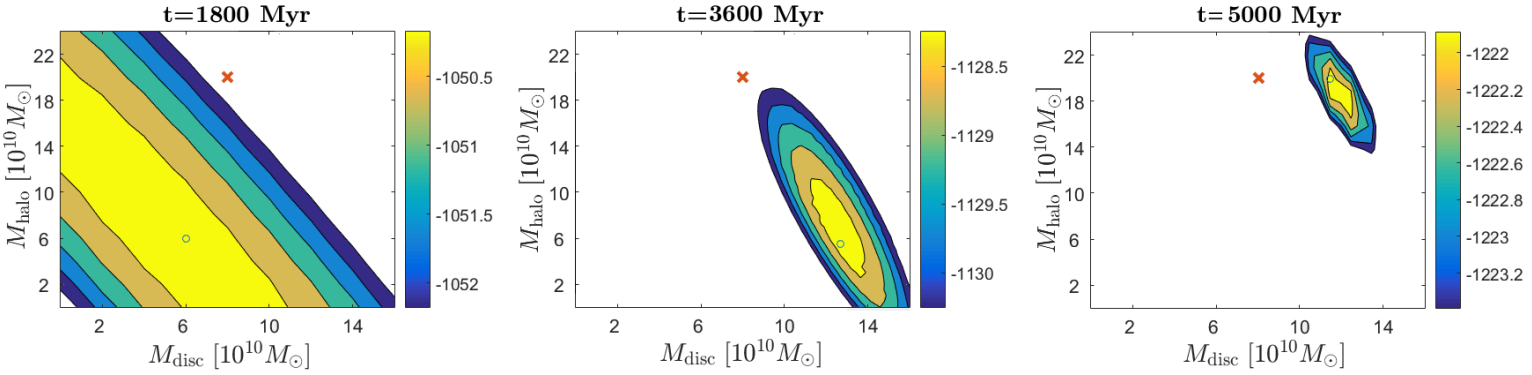

Figure 3.8: The log-likelihood plots of a stream, showing how the CR area decreases with time.

From observing the different CRs, they can be seen to have a characteristic inclination, which comes from the fact that the total mass within the region of the stream must be almost constant. This is because the total mass is roughly what dictates the curvature of the orbit. If the disc mass is altered then the halo mass must be changed accordingly, in order for an orbit to be similar to the best fit orbit. This is the linear relation seen in the CRs.

3.3.4 Testing 90% CR

This section is dedicated to determine how often the actual masses are inside the CR, so that I can include streams which are very distant from the positive mass region. Therefore, Table 3.4 only presents if the streams are in the 90% CR or not, for the entire range of initial angles and velocities considered.

Table 3.4: Data for whether streams' 90% CR contain the actual masses. The streams presented were created at $r_0 = 12$ kpc and with a range of initial velocities and angles. The data for streams created with the velocity $v_0 = 1.2v_c$ are shown in Table 3.3.

v_0 [v_c]	θ [°]	t [Myr]	In 90% CR?
0.9	15	300	Yes
		800	No
		1300	No
	30	300	Yes
		800	No
		1300	No
	45	300	No
		500	No
		700	No
		800	No
		1000	No
	60	300	No
		800	No
	75	300	Yes
		940	No
1.0	15	600	No
	30	600	Yes
		950	No
	45	600	No
		650	Yes
		700	No
		800	No
		950	No
		1050	No
		1300	No
	60	600	No
		640	No
		670	Yes
	75	600	No
		700	Yes
		1000	No
1.1	15	300	Yes
		800	No
		1300	No
	30	600	No
		1000	No
	45	600	No
		800	No
		1000	No
		1300	No
	60	600	No
		800	Yes
		1000	No
	75	600	Yes
		800	No
1.3	15	600	Yes
		1000	No
	30	600	Yes
		1000	Yes
		1300	No
	45	600	Yes
		1000	No
		1250	No
	60	600	No
		1000	Yes
		1300	No
	75	600	Yes
		800	No
		1300	No

In addition to this Table, I also use data from the tables above (3.1, 3.4 and 3.2) to draw conclusions. The few CRs that have the true values are mostly streams which are early in their formation, with a large area and peak values far-off the actual masses. Therefore, they do not necessarily confirm the orbital approximation, the CR merely has a high uncertainty and many masses give a sufficiently good fit. Despite this, they are still counted when determining the ratio of streams which have a CR with the actual value

inside them. Using the data from all the streams, the ratio of streams is determined to be $23/105 \approx 21.90\%$. If I choose to only look at streams with a CR that does not get cut off, the streams that qualify must either have a small CR area or be far away from zero mass values (these two conditions must be balanced). Doing this, I get the ratio $4/32 \approx 12.50\%$. The ratio decreases since this approach gets rid off most early streams, which have a very large CR area that, usually, includes the actual masses.

3.4 Trying to Fit with Scale Radius

The scale radius of the halo was considered to be treated as a free variable, but fitting to three parameters complicated the simulation further. Considering the scale radius meant an increase in the simulation time and constraining the parameters with a 3D CR would be difficult. It was briefly used as a free variable to fit some streams, but the scale radius was found to not have as a big impact on the fitting as the halo and disc mass (unless changed drastically). Also, it can be seen from the Hernquist potential, Eq.(2.2), to mostly be important when the distance of the stars to GC is smaller than or close to the scale radius. Therefore, the scale radius was not altered during the fitting.

Chapter 4

Conclusions

In this project, I have created a program to produce a variety of streams in a potential model which resembles the Milky Way's potential. By fitting orbits to the streams, I have analysed the viability of the orbital approximation for stellar streams using a 90% CR. From the figures and data in the tables presented, I mainly find evidence which opposes the orbital fitting method. Already when beginning the simulations and forming orbits for test particles it became evident that the simulated stars did not follow the same orbit and that the orbital approximation does not contain all of the stream stars. A significant part of streams gave CRs with a large part of their area in the negative mass region, which is unphysical; further proof against the orbit fitting method. When evaluating the ratio of CRs with the actual value inside them I found that for all streams presented I get a ratio 21.90% of streams. A more selective evaluation, only including streams with a CR entirely inside the positive mass region, yields a ratio of 12.50%. These ratios do not correspond to the 90% expected from applying a 90% CR. My key conclusion after observing all of this is that the orbital approximation is severely inaccurate and can not be used for stellar streams.

The method of fitting an orbit to streams has been used before, e.g. by Koposov et al., to constrain the potential of the Milky Way. In this project, I have tried constraining the mass of the Galaxy and shown this method to be incorrect. The error of this approximation, of course, carries on to the results, giving you inaccurate values. It is crucial for the approximation to be recognised as faulty and effort put into other, more reliable, methods. The scientific importance of accurately determining the total mass of the Galaxy lies in establishing whether the Milky Way is a typical galaxy for its mass. Several questions in cosmology depend on knowing this, e.g. the missing satellites problem, and it is impossible to ascertain if the Galaxy is typical before knowing its total mass.

The best fit for the simulated stream in Figure 3.5 further showed that it is very difficult to achieve a good fit (which includes most stream stars) when taking into consideration the orbit of one of the stream stars. Figure 3.4 demonstrated that even when the orbital approximation appears acceptable by sight, a statistical analysis finds a different best fitting mass, with a confidence region which does not contain the actual mass values. However, it should be noted that the fitting is done in 3D while the image is in 2D. The

difference between actual and best fit masses can be expected to be due to the offset of the orbit in the z-coordinates. This is in accordance with a change in mass ratio (between halo and disc) mostly affecting the z-direction, since the halo is spherical and disc close to flat (lying in the x-y plane). The CR is extended along a line in the halo mass - disc mass plane which corresponds to a constant combined mass contained within some radius (probably the typical Galactocentric radius of the stream) and the actual masses almost fall on this line, but they are still not in the 90% CR because the mass ratio is wrong. This can be related to one of the main results found by Koposov et al., they claimed to have determined the flattening of the total potential, the axis ratio in z-direction. The mass ratio, as it affects the z-direction, is similar to this and the example presented in the figure tells us that also this result by Koposov et al. is not accurate.

Among my main conclusions, I also found a few relations between stream parameters. Most noticeable is the decrease of the CR area as the time is increased. This sounds logical, since the stream gets more dragged out with time, meaning it gets thinner and fitting an orbit to it gives more precise results. Since young streams therefore give very large CRs (using this model) it seems likely that the same will be true even with better approximations. They are therefore unlikely to be useful for learning about the potential. A few streams had an increase in the CR area at some integration times, which just shows that the stream most likely became wider at some points (e.g. from passing through the disc). The random generation of the position and velocity dispersion affect the CR in unpredictable ways, but is diminished with increased particles and integration time. Other relations are observed for streams created with other initial conditions (mainly angle and velocity), but can not be confirmed from the tables. It is possible that the random effects outweigh the minor changes I observed.

There are other assumptions that I have made while analysing the orbital approximation. Most notably, cutting off the CR for negative mass values. I tried to rectify this by determining the ratio of streams described by the orbit fitting method only for CR inside the positive mass region and compare with the total ratio. However, I recognise that further analysing of CRs in the positive mass region could be done so to avoid making the "cut-off" approximation. When doing so, I would recommend using long integration times, so to decrease the area of the CR. I also assumed that for each ℓ there is only one b and r value, which implies that there is only one star per ℓ coordinate. Evidently this can cause issues during the fitting process. The assumption of single-event disruption is usually not the case in reality and could be improved in this project by, instead of releasing all particles at once, releasing them over time as the satellite is orbiting. Interaction between the simulated stars was considered a fair assumption because it is not a substantial effect during the stream creation phase of a disrupted satellite. Of course, implementing interaction would make the stream model more realistic, but would require quite a bit of computing power. The velocity of the central particle in the satellites created were assumed to be known exactly, which can be justified by the fact that the satellite's average velocity (equivalent to the central particles velocity) can be determined accurately from combining observational data from many stars. This saves us from having to add the velocity as another variable, but in reality a range of values should be considered. Lastly, the velocity

dispersion was added in this project to simulate a satellite and because we assumed to not know the exact velocities of any other particle. If one accurately knows the velocities for some streams stars, this data could be added to improve the model for real streams. They could also have been used in the simulation, where we know these values exactly.

The orbit fitting method should not be applied on stellar streams. However, there are other methods which allow for accurate stream models. First off are N-body simulations, which incorporate the interaction between bodies and produces realistic models. Unfortunately, they are computationally expensive and, therefore, unfit for investigating a large quantity of parameters. Another approach to forming stream models is the use of streaklines, a concept from fluid dynamics used to visualise flow. Streaklines are created by releasing test particles with a slight difference in position and velocity from an orbiting satellite. The particles are released at a constant time interval while the satellite and particles orbit (Küpper et al. 2012). A second example of methods uses the distribution of orbital frequencies to place stars at different positions and velocities near a similar starting point: thus, creating a stream. The orbital frequencies vary slightly, which corresponds to the different positions and velocities. This method was first applied by Bovy et al. (2016), having been proposed by Bovy (2014).

All of my code used has been uploaded to github and can be found on this webpage: `https://www.github.com/13ET/Analysing-Stellar-Streams`

Bibliography

Belokurov, V., Zucker, D. B., Evans, N. W., et al. 2006, ApJ, 642, L137

Binney, J. & Tremaine, S. 2008, Galactic Dynamics, 2nd edn. (Woodstock, Oxfordshire: Princeton University Press), 70–71

Bovy, J. 2014, ApJ, 795, 95

Bovy, J., Bahmanyar, A., Fritz, T. K., & Kallivayalil, N. 2016, ApJ, 833, 31

GAIA-ESO Website. 2013, Halo substructure, Dark Matter, extreme stars, `https://www.gaia-eso.eu/science/halo-substructure-dark-matter-extreme-stars`

Grillmair, C. J. 2006, ApJ, 645, L37

Grillmair, C. J. & Dionatos, O. 2006, in Bulletin of the American Astronomical Society, Vol. 38, American Astronomical Society Meeting Abstracts #208, 123

Hernquist, L. 1990, ApJ, 356, 359

Ibata, R., Irwin, M., Lewis, G., Ferguson, A. M. N., & Tanvir, N. 2001, Nature, 412, 49

Ibata, R. A., Gilmore, G., & Irwin, M. J. 1995, MNRAS, 277, 781

Johnston, K. V., Law, D. R., & Majewski, S. R. 2005, ApJ, 619, 800

Klypin, A., Kravtsov, A. V., Valenzuela, O., & Prada, F. 1999, ApJ, 522, 82

Koposov, S. E., Rix, H.-W., & Hogg, D. W. 2010, ApJ, 712, 260

Küpper, A. H. W., Lane, R. R., & Heggie, D. C. 2012, MNRAS, 420, 2700

Law, D. R., Johnston, K. V., & Majewski, S. R. 2005, ApJ, 619, 807

Lindegren, L. 2014, Dynamical Astronomy, Lecture Notes for ASTM13 (Lund, Skåne: Media-Tryck)

Lindegren, L. 2016, ASTM21, Statistical Tools in Astrophysics: Lecture Slides Ch. 5

Madau, P., Diemand, J., & Kuhlen, M. 2008, ApJ, 679, 1260

MathWorks Website. 2017, ode45, `https://se.mathworks.com/help/matlab/ref/ode45.html`

Moore, B., Ghigna, S., Governato, F., et al. 1999, ApJ, 524, L19

Newberg, H. J., Yanny, B., Rockosi, C., et al. 2002, ApJ, 569, 245

Phillips, S. 2005, The Structure & Evolution of Galaxies (Chichester, West Sussex: John Wiley & Sons Ltd), 19–21, 158, 160–162

Appendix A

Additional Stream Values

A.1 Number of Particles

Table A.1: The relevant parameters for streams created at $r_0 = 12$ kpc with constant angle $\theta = 45°$ and initial velocity $v_0 = 1.2v_c$. The masses presented are for the peak log-likelihood.

# particles	t [Myr]	CR area	$M_{\rm disc}$ $[10^{10}M_\odot]$	$M_{\rm halo}$ $[10^{10}M_\odot]$
50	1000	600	-7	55
		650	10	11
		1050	9	36
		540	-3	50
		525	2	23
		1500	10	56
100	1000	300	-5	50
		480	7	23
		525	3	31
		600	3	28
		345	8	15
		465	11	12
		400	2	53
	1400	10.0	8.5	21.0
		8.3	8.5	22.5
		8.5	9.0	17.0
200	1000	440	4	27
		300	5	35
		420	8	27
		180	-3	37
		150	-2	35
	1400	5.5	9.0	17.0
		3.3	7.5	26.0
		5.0	10.0	24.0
500	1000	240	5	29
		330	1	59